Fusion Based MR Images Denoising Technique Using Frequency Domain and Non-Local Means Filters

CHRISTIAN RUDAHUNGA*, HENRY KIRAGU, MARY AHUNA
Department of Electrical and Communication Engineering
Multimedia university of Kenya
P.O.BOX 15653-00503,Nairobi,
KENYA

Abstract: - The non-invasive and non-ionizing properties of Magnetic Resonance Imaging (MRI) in addition to the associated good image quality as well as high resolution make MRI more attractive than many other medical imaging techniques. However, during the acquisition, transmission, compression and storage processes, the Magnetic Resonance (MR) images are corrupted by various types of noise and artifacts that degrade their visual quality. Most of the existing MR images denoising techniques give good quality images only when the noise density is low with their performances deteriorating as the noise power increases. The few methods that yield high quality images for all noise densities involve multiple complex and time-consuming processes. This paper proposes a computationally simple MR images denoising technique that consistently gives good denoising results for low as well as high noise densities. The proposed procedure fuses an MR image that is denoised by a Modified Discrete Fast Fourier Transform (MDFFT) filter with one that is denoised using a non-local means filter in frequency domain to yield a high quality output image. The main contribution of this proposed method is the employment of a novel image fusion approach that greatly improves the quality of the denoised image. The performance of the proposed technique is compared with those of the Wiener, median, adaptive median and the MDFFT filters. Objective metrics such as the Peak Signal-to-Noise Ratio (PSNR) and the Structural Similarity (SSIM) index were used in the performance assessments. The outcomes of these assessments showed that the proposed algorithm yielded images of higher quality in terms of the PSNR measure than the existing denoising techniques by at least 7.11 dB for a noise density of up to 0.5.

Key-Words:-MRI, Denoising, Noise, Artifacts, Non-local means filter, Modified discrete fast Fourier transform.

Received: March 28, 2021. Revised: August 12, 2022. Accepted: September 18, 2022. Published: October 4, 2022.

1 Introduction

Magnetic Resonance Imaging (MRI) is one of the most efficient imaging techniques for medical diagnostics because of its non-invasive and non-ionizing capabilities [1]. However, the Magnetic Resonance (MR) images are corrupted by various noises such as Gaussian, salt and pepper and Rician noise in addition to artifacts that degrade the images. These noises and artifacts make it difficult to extract the useful information for human interpretation or computer- aided clinical analysis of the images [2]. In the development of medical imaging, various denoising techniques have been developed but the challenge of maintaining a good filtering performance as the noise amount increases still persists.

The process of noise removal must not degrade the useful features in an image. In particular, the edges are important features for medical images and thus the denoising must be balanced with edge preservation [3]. The choice of the denoising technique to be used is based on either the amount and type of noise or the performance of the filter itself. The objective of this paper was to develop and test the performance of a proposed robust denoising method for MR images. The technique fuses the output of a low pass modified fast Fourier transform filter with that of a spatial domain high pass non-local means filter.

Ali compared the performances of the median, adaptive median and adaptive Wiener filters in removing Gaussian noise as well as salt and pepper noise from MRI images. To evaluate the performance of each of the three filters, noise with densities ranging from 10% to 90% was gradually added to ground-truth MR images. Then, the Peak Signal-to-Noise (PSNR) for every filter output and for every noise density was calculated [4]. The results showed that the adaptive Wiener filter has a poor performance in removing both salt and pepper and Gaussian noises from the images. The median filter was the best in removing Gaussian noise. The adaptative median filter was better than both the median and adaptive Wiener filters in removing the salt and pepper noise. However, all the three filters showed poor performance for high noise densities.

In order to improve denoising performance, Sarker et al. combined the adaptive median filter and the

non-local means filter algorithms to remove salt and pepper noise from MR images. Salt and pepper noise with a variance ranging from 0.1 to 0.9 was added to ground-truth MR images prior to denoising. The PSNR values of the denoised images for median, adaptive median as well as the adaptive median-based non-local means filters, at a noise variance equal to 0.9 were 54.12 dB, 56.80 dB and 58.70 dB respectively[5]. Therefore, a combination of the adaptive median filter and the non-local means filter performed better than both the median filter and adaptive median filters. The main limitation of this combined filters denoising technique is the long processing time required because it is a two-stage method that involves a large number of computations [5].

These related works reveal two challenges. On one hand, the filters perform well at low noise densities and poorly at higher noise densities. On the other hand, the combination of adaptive median filter and non-local means filter algorithm proved to be good for both low and high noise densities but its operation takes a long processing time. To address these gaps, fusion of the outputs of a Modified Discrete Fast Fourier Transform (MDFFT) filter algorithm and a Non-Local Means Filter (NLMF) was employed in the method proposed in this paper. The MDFFT algorithm denoises the low frequency components of the MR images while the NLMF was used to denoise the high frequency components of the same image. In order to reconstruct the denoised MR image, the outputs of the two filter algorithms were fused in the Discrete Fourier Transform (DFT) domain. The main contribution of this research work is a proposed frequency domain-based image fusion technique that yields better quality images than conventional image fusion methods. The image fusion used in this paper selects the high frequency components from the high pass filtered image and discards the still noisy low frequency components of high pass filtered image. From the output of the low pass filter, the low frequency components are selected while completely removing the high frequency ones. This is followed by combining the selected high and low frequency components to reconstruct the denoised image in frequency domain. This proposed fusion procedure results in a better output quality than the conventional image fusion techniques that are based on combining scaled versions of the inputs and therefore retaining significant amounts of noise power in their fused images. The rest of this paper is organized as follows: section 2 presents some background theory on MRI principles, image denoising techniques and image quality measures. Section 3 gives a presentation of the proposed methodology. Simulation test results and their discussions are presented in section 4 while section 5 gives the conclusion and suggestions for future research.

2 Theoretical Background

This section summarizes the principles of the MRI process. Some types of the noises and artifacts that corrupt the MR images are discussed. Also, objective measures that are commonly used to assess the quality of MR images are presented here.

2.1 Magnetic Resonance Imaging

The Magnetic Resonance Images (MRI) technique is based on the phenomenon of nuclear magnetic resonance of the hydrogen nuclei contained in the human body in form of water, fat and other chemical components [6]. It is a powerful tool for imaging the structure and the function of soft tissues in the human body because of its high image contrast and resolution capabilities as well the absence of ionizing radiations and the ability of arbitrary spatial encoding [7]. The abundance of hydrogen in the human body coupled with its solitary proton per atom leads to the generation of large values of net magnetization in the body. When nuclei of certain elements are placed in a magnetic field, they absorb energy in the Radio Frequency (RF) range of electromagnetic waves and emit that energy while returning to their initial state [8]. In the absence of an external magnetic field, the magnetic moments (μ) of the hydrogen protons in a body tissue are oriented randomly in all directions. Consequently, the net magnetic moment (magnetization) is equal to zero as shown in the following equation [9].

$$\vec{M} = \sum \vec{\mu} = 0 \qquad (1)$$

Where $\vec{M}$ is the net magnetization.

In the presence of an external static magnetic field $\overrightarrow{B_0}$, the magnetic moments are oriented in the longitudinal direction of $\overrightarrow{B_0}$ and rotate (precess) around $\overrightarrow{B_0}$ at the Larmor frequency f_0 given by;

$$f_o = \frac{\gamma}{2\pi}\overrightarrow{B_0} \qquad (2)$$

where γ is the gyromagnetic ratio of the precessing nucleus [10]. During the precession, the longitudinal component of the magnetization (M_z) remains constant whereas its transverse component ($\overrightarrow{M_{XY}}$) is zero.

2.1.1 RF Excitation and MR Image Formation

In MRI, an RF pulse is used to flip some of the magnetization into the transverse plane. The precession motion is then transformed into a spinning motion of the nucleus around the axis of the static magnetic field. Application of RF pulses that have a frequency equal to the Larmor frequency lead to the decrease of longitudinal magnetization ($\vec{M}z$) and the creation of transverse magnetization component ($\overrightarrow{M_{XY}}$). The net magnetization ($\vec{M}$) continues to revolve around the magnetic field $\overrightarrow{B_0}$ at the Larmor frequency but with a tilt angle (α) that is proportional to the RF pulse duration time (τ). At the end of RF pulse application, the transverse magnetization component ($\overrightarrow{M_{XY}}$) starts to decrease towards its minimum value whereas the longitudinal magnetization starts to increase towards its maximum value. The increase in longitudinal component of magnetization $\overrightarrow{M_Z}$ when returning back to its equilibrium value M_0 is called longitudinal relaxation which can be expressed as follows;

$$M_Z(t) = M_0\left(1 - e^{-t/T1}\right) + M_Z(0)e^{-t/T1} \quad (3)$$

Where T_1 is the longitudinal relaxation time constant, M_0 is the equilibrium magnetization, $Mz(0)$ is the longitudinal instantaneous magnetization after pulse excitation [11].

The decay of the transverse magnetization $\overrightarrow{M_{XY}}$ is called transverse relaxation given by;

$$M_{XY}(t) = M_{XY}(0)e^{-t/T2} \quad (4)$$

Where T_2 is the transverse relaxation time constant and $Mxy(0)$ is the instantaneous transverse magnetization after pulse excitation [11]. The collapsing of the transverse magnetization component induces an electric voltage in the receiver coil of the MRI equipment. This induced signal is called the Free Induction Decay (FID) signal given by;

$$S(k_x, k_y) = \int_{\frac{-F_Y}{2}}^{\frac{F_Y}{2}} \int_{\frac{-F_X}{2}}^{\frac{F_X}{2}} M(x,y)e^{-j2\pi[k_x(t)x + k_y(t)y]}\, dx\, d; \quad (5)$$

Where $S(k_x, k_y)$ is the FID signal, $k_x(t)$ and $k_y(t)$ are the spatial frequency components in the read-out and phase -encoding directions respectively. Fx and Fy are the fields of view in x and y directions respectively [12]. The MR image is obtained by evaluating the two-dimensional inverse Fourier transform of the FID signal.

2.1. 2 MRI Noises

Magnetic resonance images are prone to various types of noise that degrade their quality. These noises include the Gaussian noise and the salt and pepper noise. Gaussian noise is a random noise that has the following normal probability density function(pdf)

$$P(x) = \frac{1}{\sigma\sqrt{2\pi}} e^{\frac{-(x-\mu)^2}{2\sigma^2}} \quad (6)$$

where $P(x)$ is the Gaussian noise pdf, μ is its mean and σ is its standard deviation [13].

The salt and pepper noise is a random noise whose value at any position in the image is either the maximum intensity level (salt value) or the minimum one (pepper value) [14]. It manifests itself as dark and bright spots in the image and has the following probability density function.

$$P(x) = \begin{cases} p_a, & for\ x = a \\ p_b, & for\ x = b \\ 0, & otherwise \end{cases} \quad (7)$$

where $P(x)$ is the salt and pepper noise pdf while p_a and p_b are the values of the pdf for the intensity levels a and b respectively [5].

2.1.3 Types of MRI Artifacts

Image artifacts refer to any image features that are not inherently present in the imaged scene. They lead to misinterpretation of medical information in MR images [15]. Some of the artifacts associated with MRI are: truncation, motion, aliasing and chemical shift artifacts. The sources of these artifacts include: body motion, magnetic field inhomogeneities, body chemical state shift and image processing techniques used. Truncation artifacts occur at the boundaries with sharp contrast in the form of multiple alternating bright and dark lines. For example, the symmetric truncation in k-space leads to the oscillations of sampled data or Gibbs-ringing artifacts around the boundaries of the tissue[16] .They can be misinterpreted as a syrinx in the spinal cord or a mechanical tear in the knee [17]. Motion artifacts originate from the various movements in the body parts of the patient such as the lungs and heart during the MRI process. Aliasing artifacts affect the MR images when the Field of View (FoV) is small. They result in some body parts that are outside the FoV being mapped at the opposite end of the image. The chemical shift artifacts appear like dark and bright bands at the interface between lipid and water. These artifacts are sometimes helpful as a diagnostic aid for confirming the presence of fat within lesions [17].

2.2 Spatial Domain Filtering Method

Spatial domain filtering can be categorized into linear and non-linear methods [18]. The linear filters such as the mean and maximum filters operate in spatial and temporal domain. They reduce the noise by changing the value of each pixel based on the values of the pixels in its neighborhood. The problem associated with these filters is that they blur the image edges and other fine details. The non-linear filters such as the median and non-local means filters are more preferred over the linear ones because they reduce noise and also preserve the image edges and boundaries [19]. Despite the advantageous features of non-linear filters, they still suffer from serious drawbacks such as blurring of the filtered images.

2.2.1 Non-Local Means Filter

The operation of a Non-Local Means (NLM) filter is based on estimating the intensity of each pixel from the information obtained from the entire image. It exploits the redundancy due to the presence of similar patterns and features in the image [2]. The weight *W(m,n)* assigned to a pixel is proportional to the similarity between the local neighborhood of the pixel under consideration and the neighborhood corresponding to other pixels in the image. The limitation of non-local means filter is that the denoised image is affected by the blurring due to appearance of the artifacts in the smooth regions of filtered image and loss of the fine details when the amount of noise becomes high [20]. For a pixel *n* in the image *I,* corrupted by noise of value $v=v(n)|n \in I$ the estimated value of that pixel denoised by a non-local means filter, LM[$v(n)$], is calculated as a weighted average of all pixels in the image.

The weight, *W(m,n),* depends on the similarity between the pixels *m* and *n* as shown in the following equation [18].

$$NLM[V(n)] = \sum_{n \in I} W(m,n)V(n) \quad (8)$$
$$\text{with } 0 \leq W(m,n) \leq 1$$

The advantages of spatial domain filters are their simplicity as well as the ability to operate in real time. Their shortcomings include lack of robustness and the imperceptibility of their filtering effects. The frequency domain filters can be used to address these challenges associated with spatial domain filters [21].

2.3 Frequency Domain Filters

In frequency domain filtering, the image to be denoised is first transformed into frequency domain by evaluating it two-dimensional Discrete Fourier Transform (2D-DFT) [22].

Filtering is then achieved by multiplying the frequency domain image by the transfer function of an appropriate filter. The MR image to be denoised in frequency domain is first divided into spectral bands and the filtering mechanism is applied to each of these bands [23]. Finally, two-dimensional Inverse Discrete Fourier Transformation (2D-IDFT) is performed on the product to obtain the filtered image in spatial domain. One of the advantages of frequency domain filtering is the ability to concentrate most of the signal energy in the low frequency components allowing easy removal of high frequency noise. Other merits of these filters are their low computation complexity as well as the ease of visualizing and manipulating the image in frequency domain. The challenges associated with the frequency domain filtering are image blurring as a result of low pass filtering as well as image over-sharpening by high-pass filters. One of the commonly used frequency domain filters is the Gaussian low-pass filter whose transfer function is given by;

$$H(u,v) = e^{\frac{-D^2(u,v)}{2D_o^2}} \quad (9)$$

where *H(u,v)* is the transfer function of the filter, *Do* is a constant and *D(u,v)* is the two dimensional spatial frequency [22].

2.4 Objective Quality Measures

Two of the widely used objective measures for assessing the quality of an image are the Peak signal-to-Noise Ratio (PSNR) and the Structural similarity (SSIM) index.

2.4.1 Peak Signal-to-Noise Ratio (PSNR)

The Peak Signal-to-Noise Ratio is an objective measure that is obtained by dividing the maximum possible power of the ground-truth image by the mean squared power of the noise in the denoised image. In digital images processing, the PSNR metric considers the Mean Squared Error(MSE) between the ground-truth or original image and the denoised image [24]. It is usually expressed in decibels as follows;

$$PSNR = 10log_{10}\left(\frac{(MAX)^2}{MSE}\right) \quad (10)$$

Where *MSE* is mean squared error and *MAX* is the maximum pixel intensity value [25].

2.4.2 Structural Similarity (SSIM) Index

The SSIM of an image is a quality assessment measure that is widely used for quality evaluation in images processing. It compares the similarity between two images. This metric quantifies the difference between a degraded image and the ground-truth image based on the luminance, structure and contrast of the two images [26]. The SSIM is calculated as follows;

$$SSIM(x,y) = \frac{(2\mu_\chi\mu_\gamma + C1)(2\sigma_{\chi\gamma} + C2)}{(\mu_\chi{}^2 + \mu_\gamma{}^2 + C1)(\sigma_\chi{}^2 + \sigma_\gamma{}^2 + C2)} \quad (11)$$

Where μ_χ is the mean of the pixel values of the reference image (x). μ_γ is the mean of the pixel values of the degraded image (y). σ_χ and σ_γ are the standard deviations of the pixel values of the reference image and the degraded image respectively. C1 and C2 are constants to ensure that the value of the SSIM is always finite [12].

3 Methodology

The proposed MR image denoising technique presented in this section is composed of the stages shown in Fig. 1. The algorithm separately denoises a noisy image using both a frequency domain Gaussian low pass filter and a spatial domain high pass non-local means filter. Since the Gaussian filter denoises low frequency components better than it does for higher frequency ones, its denoised low frequency components are extracted to form the low frequency part of the denoised output image of the algorithm. On the other hand, the non-local means filter, denoises the higher frequency components better than lower frequency ones. The high frequency components of the output of this filter are extracted to constitute the high frequency components of the denoised output image. The extracted low and high frequency components are then combined by matrix summation to reconstruct the denoised output image.

The process of extracting and fusing the frequency components to reconstruct the denoised image was carried out using the following procedure. Salt and pepper or Gaussian noise was added gradually (variance between 0.1 to 0.9) to a $P \times Q$ pixels ground-truth image, $A(m, n)$ to form a noisy image, $A_N(m, n)$ as follows;

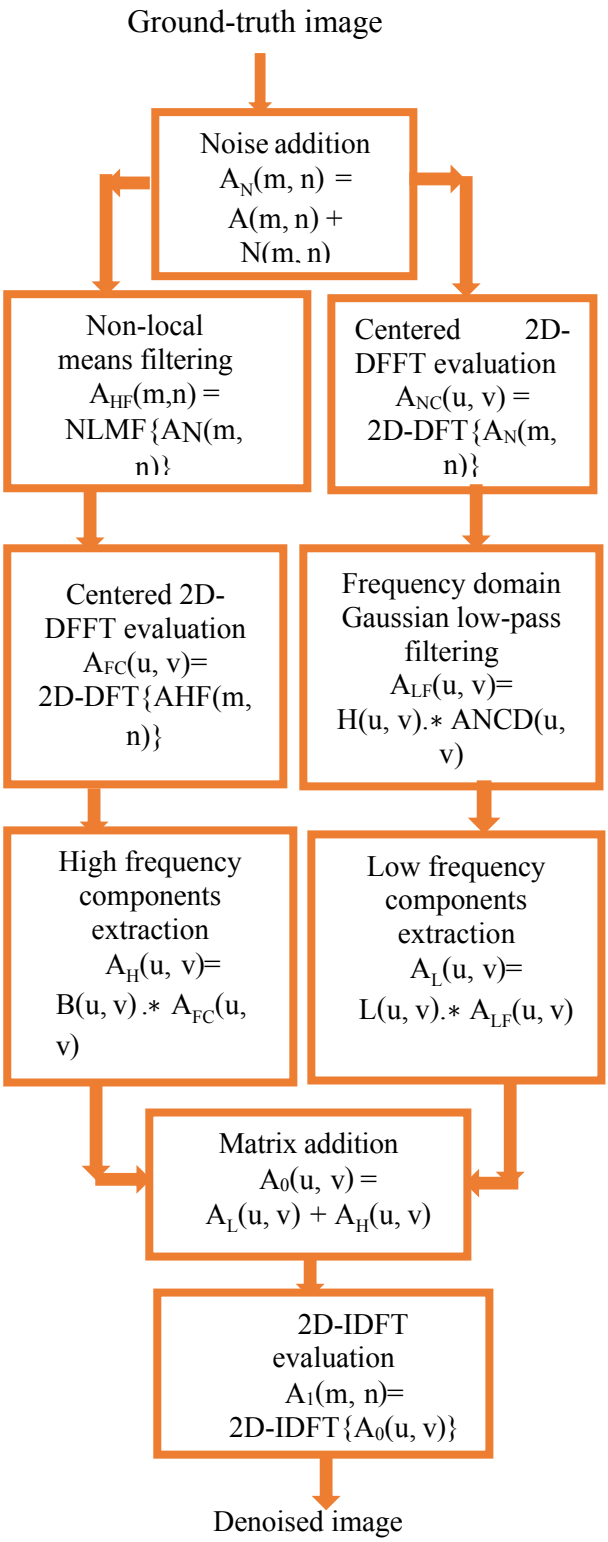

Fig. 1: Flowchart of the proposed method.

$$A_N(m,n) = A(m,n) + N(m,n) \quad (12)$$

Where $N(m,n)$ is an $P \times Q$ noise matrix, $1 \leq m \leq P$ and $1 \leq n \leq Q$. The noisy image was then transformed into frequency domain by taking its two-dimensional Discrete Fourier Transform (2D-DFT).

The 2D-DFT was centered in order to put the low frequency components of the noisy image at the center of matrix $A_{NC}(u,v)$ as follows;

$$A_{NC}(u,v) = 2D - DFT\{A_N(m,n)\} \quad (13)$$

Where $1 \le u \le P$, $1 \le v \le Q$ and $2D - DFT\{.\}$ denotes the centered 2D-DFT. The centered frequency domain image was low pass filtered by multiplying it element-wise by the transfer function of a Gaussian low pass filter as follows;

$$A_{LF}(u,v) = H(u,v).* A_{NCD}(u,v) \quad (14)$$

Where {.*} denotes element-by-element matrix multiplication, $A_{LF}(u,v)$ is the low pass filtered image in frequency domain and $H(u,v)$ is the transfer function of the modified Gaussian low pass filter given by;

$$H(u,v) = H_O e^{-\frac{cD^2(u,v)}{2D_0^2}} \quad (15)$$

Where H_0, c and D_0 are constants while $D(u,v)$ is the two-dimensional spatial frequency given by;

$$D(u,v) = \sqrt{\left(\left(u - \frac{P}{2}\right)^2 + \left(v - \frac{Q}{2}\right)^2\right)} \quad (16)$$

The low frequency components of the filtered image were extracted by element-wise multiplication of $A_{LF}(u,v)$ by a low pass filter mask $L(u,v)$ as follows;

$$A_L(u,v) = L(u,v).* A_{LF}(u,v) \quad (17)$$

Where $A_L(u,v)$is a matrix containing only the low frequency components of $A_{LF}(u,v)$ and $L(u,v)$ is the low pass mask defined as follow;

$$L(u,v) = \begin{cases} 1 \; for \; D(u,v) \le K \\ 0 \qquad otherwise \end{cases} \quad (18)$$

Where *K* is the highest frequency extracted by the mask. The value of *K* used was obtained as follows;

$$K = 5 \times 10^{-3}(\sqrt{P^2 + Q^2}) \quad (19)$$

The same noisy image ($A_N(m,n)$) was also denoised by the non-local means filter to produce the image $A_{HF}(m,n)$ as follows;

$$A_{HF}(m,n) = NLMF\{A_N(m,n)\} \quad (20)$$

where $NLMF\{.\}$ denotes non local means filtering. The filtered image *($A_{HF}(m,n)$)* was transformed into frequency domain by evaluating its centered 2D-DFT so that its high frequency components are at the periphery of matrix $A_{FC}(u,v)$ as;

$$A_{FC}(u,v) = 2D - DFT\{A_{HF}(m,n)\} \quad (21)$$

The high frequency components of the filtered image were extracted using element-wise multiplication of $A_{FC}(u,v)$ by a high pass filter mask $B(u,v)$ as follows;

$$A_H(u,v) = B(u,v).* A_{FC}(u,v) \quad (22)$$

Where $A_H(u,v)$ is a matrix containing only the high frequency components of $A_{FC}(u,v)$ and $B(u,v)$ is the high pass mask defined as follow;

$$B(u,v) = \begin{cases} 1 \; for \; D(u,v) > K \\ 0 \qquad otherwise \end{cases} \quad (23)$$

The 2D-DFT of the denoised image was reconstructed as matrix $A_0(u,v)$ by combining the extracted low and high frequency components as follows;

$$A_0(u,v) = A_L(u,v) + A_H(u,v) \quad (24)$$

Finally, the denoised output image was obtained by taking the two-dimensional Inverse Discrete Fourier Transform (2D-IDFT) of $A_0(u,v)$ as;

$$A_1(m,n) = 2D - IDFT\{A_0(u,v)\} \quad (25)$$

where $2D - IDFT\{.\}$ denotes the 2D-IDFT and $A_1(m,n)$ is the denoised output image.

4 Results and Discussions

The test results of the proposed algorithm are presented in this section. The results were generated by computer simulation of the algorithm using maths works MATLAB 2018a software. The test MR images were obtained from the Kenya Sonar Imaging Center and the Siemens Healthineers website [27]. The values of the constants used are: $H_0 = 1, c = 0.5,\ D_0 = 650,$ $701 \le P \le 1801\ and\ 751 \le Q \le 1851.$

To generate the results, salt and pepper or Gaussian noise was added gradually (from a variance of 0.1 to 0.9) to one of a sample of ten MR images at a time. The Peak Signal to Noise Ratio (PSNR) and the Structural Similarity(SSIM) index were calculated for every salt and pepper or Gaussian noise density and for every filter. The proposed algorithm was used to denoise the MR images and its results compared with those of other denoising techniques such as: modified discrete fast Fourier transform, median, adaptive median and Wiener filters. The comparison was done both qualitatively and quantitatively using objective measures such as the Peak Signal-to-Noise Ratio (PSNR) and the Structural Similarity (SSIM) index.

The statistical summary was used to represent graphically the denoising performance of every filter and to compare the filtering activities of all the filter algorithms.

4.1 Qualitative analysis

In Fig. 2, a subjective comparison of the performances of the proposed method to that of the modified discrete fast Fourier transform filter is presented. Column (a) shows the ground-truth $P \times Q$ pixels head MR image. Column (b) from top to bottom shows the image corrupted by salt and pepper noise of variances 0.1, 0.3, 0.5 and 0.7 respectively. More the noise density increases from top downward, more the Head MR image gets corrupted. For example, at 0.3 and 0.5 salt and pepper noise variances, the Head image is much corrupted in such way it is very difficult to recognize it. Results of denoising the noisy image using the MDFFT filter as well as the proposed algorithm are presented in columns (c) and (d) respectively. By visual observation, the proposed algorithm yielded images of higher quality than the MDFFT filter for all the noise variances tested.

In fig. 3, another subjective comparison of the performances of the proposed method to that of the modified discrete fast Fourier filter is presented. Four different MR images (Head, Ankle, Shoulder and Neck) are corrupted by salt and pepper noise. Column (a) shows four different ground-truth MR images. The images corrupted by a salt and pepper noise of variance 0.3 are presented in column (b). Results of denoising the images using the MDFFT filter as well as the proposed algorithm are presented in columns (c) and (d) respectively. By observation, the proposed algorithm produced images of better quality than the MDFFT filter.

A qualitative comparison of the performances of the proposed and the MDFFT methods for images corrupted by Gaussian noise is presented in fig. 4. Column (a) shows a ground-truth Neck MR image. From top to bottom of column (b), the MR image corrupted by Gaussian noise of variances 0.1, 0.3, 0.5 and 0.7 respectively is given. The Gaussian noise is added increasingly from top downward and more the noise density increases more the Neck MR image get corrupted. Denoising results of the MDFFT filter and the proposed algorithm are shown in columns (c) and (d) respectively. By subjective comparison, the proposed algorithm yielded images of higher quality than the MDFFT filter for low noise variances. For higher noise variances, the visual quality for MDFFT and the proposed methods are similar. This means that the denoising performance of the proposed algorithm is better than that of MDFFT filter for low Gaussian noise densities. But for high Gaussian noise densities, the denoising performances of MDFFT filter and proposed algorithm are almost equal.

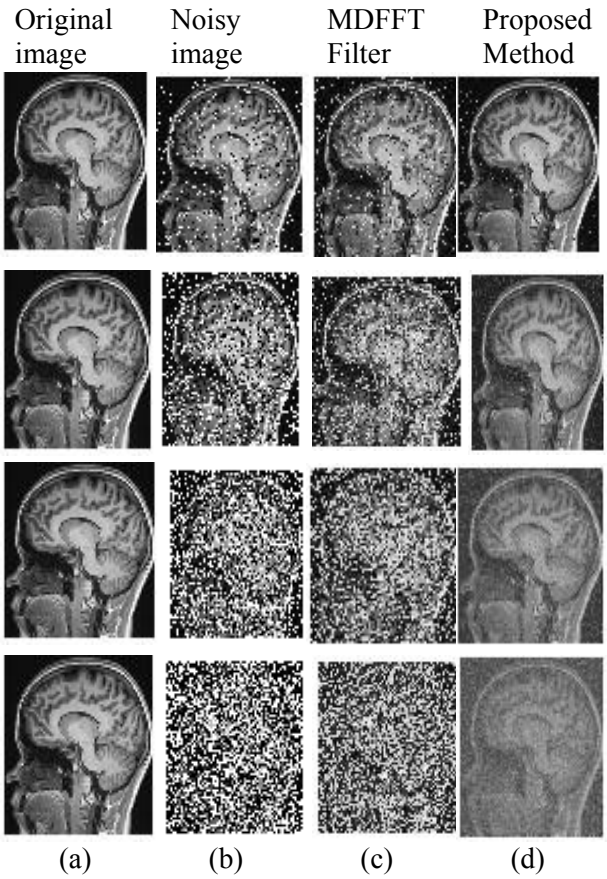

Fig. 2: Comparison between the MDFFT filter and the proposed method. (a) Original image. (b) Salt and pepper noise corrupted image. (c) MDFFT filter denoised image. (d) Proposed method denoised image.

In fig. 5, a comparison of the Gaussian noise removal capabilities of the proposed method and the MDFFT filter is presented. The MR images used are those of a Head, Ankle, Shoulder and Neck as presented in column (a). Column (b) presents the four MR images corrupted by Gaussian noise of variance 0.3. Results of denoising the noisy images using the MDFFT filter as well as the proposed algorithm are presented in columns (c) and (d) respectively. By visual observation, it was found that the proposed algorithm produced images of better quality than the MDFFT filter for low Gaussian noise variances. However, there is no perceptible difference between the noise removal efficacies of the two methods when the Gaussian noise variance is higher than 0.3. This is evident from the denoising results presented in third and fourth rows of fig. 4 for noise variances equal to 0.5 and 0.7 respectively.

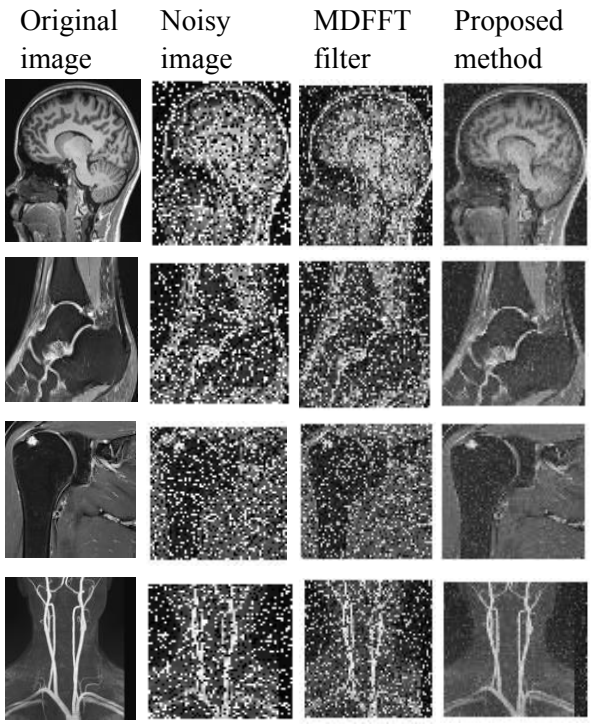

Fig. 3: Performance comparison for different images. (a) Original image. (b) Salt and pepper noise corrupted images. (b) MDFFT filter denoised image. (d) Proposed method denoised.

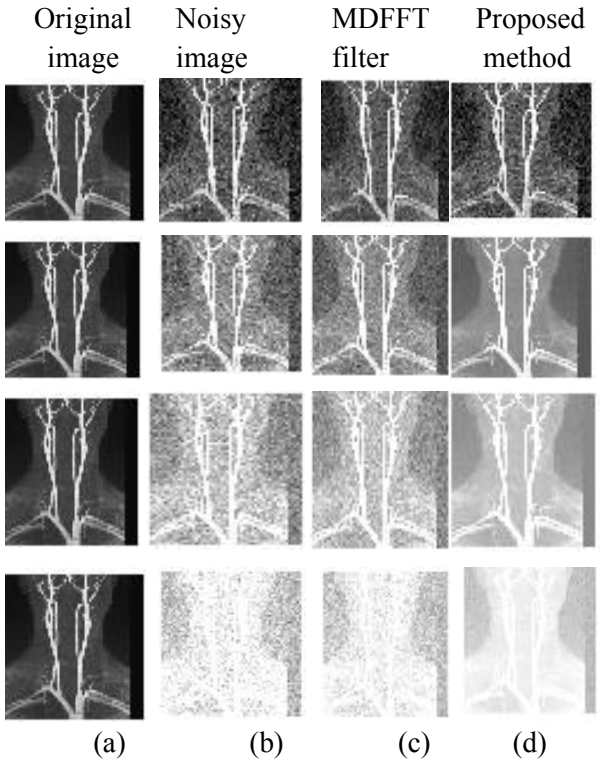

Fig. 4: Gaussian noise removal comparison. (a) Original image. (b) Gaussian noise corrupted image. (c) MDFFT filter denoised image. (d) Proposed method denoised image.

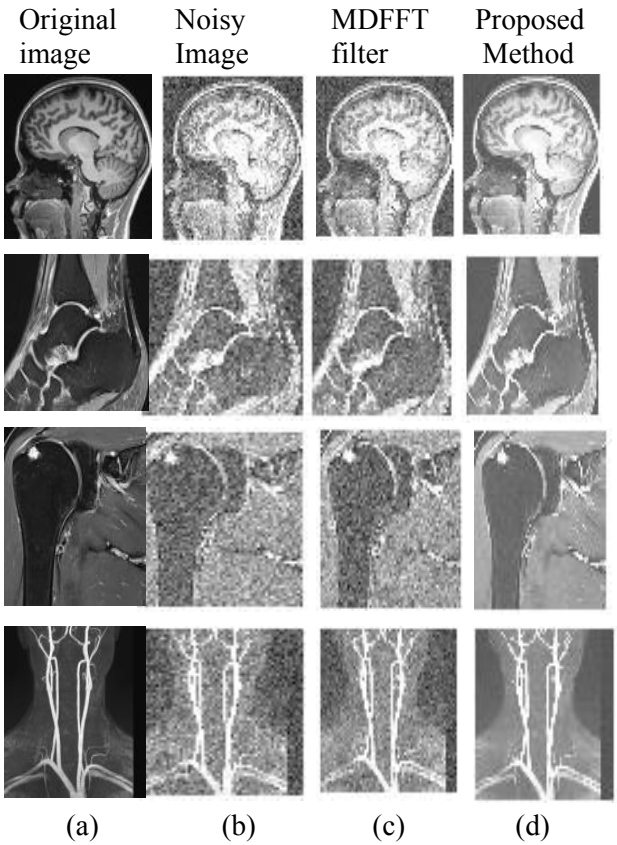

Fig. 5: Performance comparison for different images. (a) Original image. (b) Noisy image with 0.3 noise variance. (c) MDFFT filter denoised image. (d) Proposed method denoised image.

4.2 Quantitative analysis

For objective quality analysis, five filter algorithms were used to remove salt and pepper and Gaussian noises from MR images. The algorithms used are the Wiener, median, adaptive median and the MDFFT filters in addition to the proposed method. The PSNR and SSIM measures were used to compare their filtering performances. Table 1 shows the denoising performances of the five algorithms in removing salt and pepper noise in terms of the mean PSNR for ten MR images.

The proposed method produced images of higher quality than the other algorithms for both low and high noise densities (variances). For example, the mean PSNR of the proposed method is 9.73 dB and 5.72 dB higher than for any of the other filters at 0.2 and 0.7 noise densities respectively. For Gaussian noise removal, the performances of the proposed method and four other algorithms are presented in table 2 in terms of mean PSNR. The other four methods are the Wiener, median, adaptive median and the MDFFT algorithms.

The proposed method out-performs all the other four filters when the Gaussian noise density is low.

For example, at a noise of density of 0.1, the mean PSNR of the proposed method is at least 1.86 dB higher than those of the other four filters. At higher noise densities, the performance of the proposed method is comparable to that of the MDFFT filter but better than those of the Wiener, median and adaptive median filters. In terms of the SSIM index, table 3 gives a comparison of the denoising performances of the proposed method and the MDFFTF in removing salt and pepper noise. The SSIM values were averaged for ten MR images at different noise densities.

Table 1. Mean PSNR for salt and pepper noise removal

Salt and pepper noise density	Denoising algorithms				
	Wiener	Median	Adaptive median	MDFF filter	Proposed method
	PSNR in dB	PSNR in dB	PSNR in dB	PSNR in dB	PSNR in dB
0.1	45.25	61.82	66.86	64.87	71.13
0.2	42.78	58.78	62.32	61.79	72.05
0.3	40.88	56.66	59.45	59.97	69.14
0.4	39.20	54.22	57.25	58.65	66.68
0.5	37.80	52.05	54.92	57.61	64.72
0.6	36.55	49.33	52.80	56.76	63.11
0.7	35.37	46.55	50.66	56.03	61.75
0.8	34.38	43.26	45.75	55.39	60.57
0.9	33.47	39.13	40.19	54.82	59.53

Table 2. Mean PSNR for Gaussian noise removal

Gaussian noise density	Denoising algorithms				
	Wiener	Median	Adaptive .median	MDFFT	Proposed method
	PSNR in dB	PSNR in dB	PSNR in dB	PSNR in dB	PSNR in dB
0.1	43.21	51.98	38.98	66.17	68.03
0.2	40.72	50.00	36.61	61.65	62.21
0.3	39.40	48.81	35.53	58.54	58.78
0.4	38.54	47.90	34.94	56.26	56.38
0.5	37.92	47.27	34.55	54.50	54.56
0.6	37.46	46.77	34.28	53.13	53.14
0.7	37.05	46.27	34.08	52.09	52.08
0.8	36.78	45.94	33.93	51.39	51.37
0.9	36.53	45.54	33.79	50.98	50.97

Table 3. Mean SSIM for salt and pepper noise removal

Salt and Pepper noise density	Denoising algorithms	
	MDFFTF	Proposed method
	SSIM	SSIM
0.1	0.81	0.94
0.2	0.66	0.95
0.3	0.55	0.91
0.4	0.45	0.85
0.5	0.37	0.78
0.6	0.30	0.70
0.7	0.24	0.61
0.8	0.19	0.52
0.9	0.14	0.43

The proposed method yielded a better salt and pepper noise removal capability than the MDFFT filter. This superiority of the proposed method to MDFFT filter holds for both low as well as high noise densities. For example, at a noise density of 0.2, the mean SSIM indexes of the images denoised using the proposed method and MDFFT filter are 0.95 and 0.66 respectively. When the noise density is 0.8, the proposed method produced an output image with a mean SSIM index of 0.52 compared to the value of 0.19 obtained using the MDFFT filter. This is a confirmation of the mean PSNR results presented in table 1.

4.3 Statistical Summary

A statistical summary of the performance of the proposed method in comparison with other denoising methods is graphically presented in fig.6. In part (a), plots of the mean PSNR values of Wiener, median, adaptive median, MDFFT and the proposed algorithms versus the noise density of salt and pepper noise are shown. For every filter, the mean PSNR reduces as the noise density increases. The proposed method has the highest mean PSNR for all the noise densities tested. At 0.2 and 0.7 noise variances, the proposed algorithm out-performs the other four methods by at least 9.73 dB and 5.72 dB respectively. Hence, it exhibits better salt and pepper filtering performance than the other four algorithms.

(a)

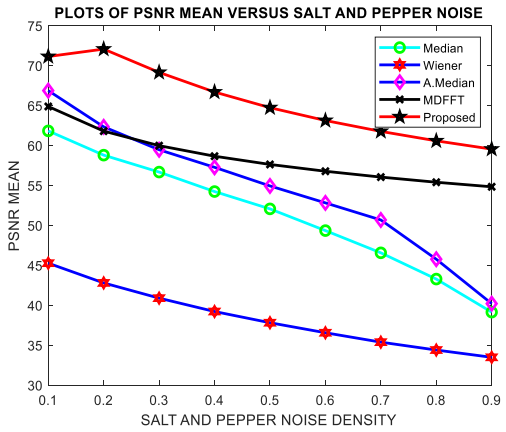

(b)

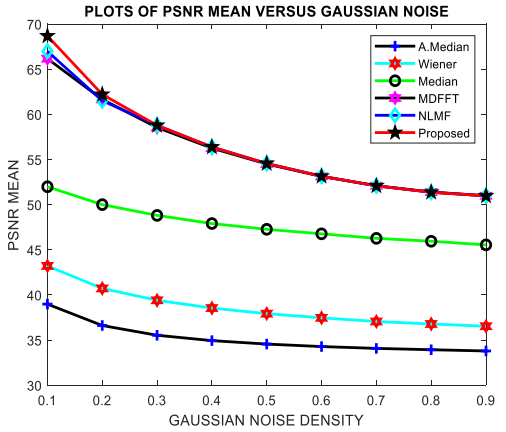

(c)

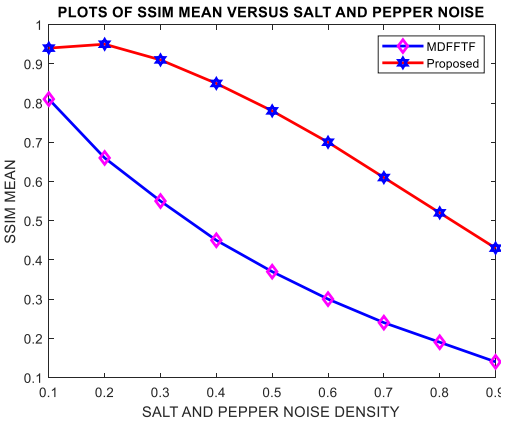

Fig.6: Statistical summary.

(a) Mean PSNR versus Salt and pepper noise density. (b) Mean PSNR versus Gaussian noise density. (c) Mean SSIM mean versus Salt & pepper density**.**

A performance comparison of the five denoising techniques for images corrupted by Gaussian noise is presented in part (b) of the figure. The mean PSNR values of the denoised images are plotted against the noise density. When the noise variance is 0.3 or lower, the proposed method portrays a better noise removal performance than the other four filters. For example, at a noise density of 0.1, the proposed method yielded a mean PSNR of 68.03 dB while all the other four methods gave PSNR values that are lower than 66.20 dB. For noise densities above 0.3, the quality performance of the proposed technique is comparable to that of the MDFFT filter but better than those of the other three filters.

In part (c), plots of the mean SSIM index versus salt and pepper noise density for the MDFFT filter as well as the proposed method are presented. The mean SSIM index values for the proposed method are higher than those of the MDFFT filter. These results reaffirm the findings of part (a) that the proposed method is superior to the MDFFT filter in removing salt and pepper noise from MR images.

5 Conclusion

In this Paper, a proposed novel MR images denoising technique has been presented. The performance of the method has been compared with the Wiener, median, adaptive median and modified discrete fast Fourier transform filters for the removal of salt and pepper as well as Gaussian noise. Objective quality assessments showed that the proposed method performed better than the others in removing salt and pepper noise for both low and high noise densities. For example, the proposed method yielded average PSNR values that were higher than those of the other filters by at least 9.73 dB and 5.72 dB for noise variances of 0.2 and 0.7 respectively. Further research work will be focused on optimizing the performance of the proposed algorithm by adjusting the parameters of the Gaussian filter.

References:

[1] Gossuin Y, Hocq A, Gillis P, Lam V. Physics of Magnetic Resonance Imaging: from Spin to Pixel. *Journal of Physics D:Applied Physics*, Vol. 43, No. 21, 2010, pp. 1-15.

[2] Yousuf M, Nobi M. A new Method to Remove Noise in Magnetic Resonance and Ultrasound Images. *Journal of Scientific Research.*, Vol. 3, No. 1, 2011, pp. 81–89.

[3] Pawar M, Sale D, DYPIT P. MRI and CT Image Denoising Using Gaussian Filter, Wavelet Transform and Curvelet Transform. *International Journal of Engineering Science and Computing*, Vol. 7, No. 5, 2017, pp. 12013–12016.

[4] Ali H. "MRI medical image denoising by fundamental filters," *High-Resolution. Neuroimaging-Basic Physical Principles and Clinical Applications*, Vol. 14, 2018, pp. 111–124.

[5] Sarker S, Chowdhury S, Laha S, Dey D. Use of Non-Local Means Filter to Denoise Image Corrupted by Salt and Pepper Noise. *Signal & Image Processing*, Vol. 3, No. 2, 2012, pp. 223-235.

[6] Kathiravan S, Kanakaraj J. A Review of Magnetic Resonance Imaging Techniques. *SmartCR*, Vol. 3, No. 5, 2013, pp. 358–366.

[7] Zhang X, *et al.* "Accelerated MRI reconstruction with separable and enhanced low-rank Hankel regularization," *IEEE Transactions on Medical Imaging*, Vol.41,No.9, 2022, pp.2487-2496.

[8] Katti G, Ara S, Shireen A. Magnetic Resonance Imaging (MRI)–A Review. *International Journal of Dental Clinics*, Vol. 3, No. 1, 2011, pp. 65–70.

[9] Moratal D, Brummer M, Martí-Bonmatí L, Vallés-Lluch A. NMR Imaging. *Wiley Encyclopaedia of Biomedical Engineering. Hoboken, New Jersey: John Wiley & Sons*, 2006, pp. 2590–2606.

[10] Fullerton G. Magnetic Resonance Imaging Signal Concepts. *Radiographics*, Vol. 7, No. 3, 1987, pp. 579–596.

[11] Odaibo G. A Quantum Mechanical Review of Magnetic Resonance Imaging. *ArXiv Preprint. ArXiv:12100946v1[physics.med-ph]*,2012,pp.1-54.

[12] Kiragu H, Mwange E, Kamucha G. A Novel Compressive Sampling MRI Method Using Variable-Density k-Space Under-sampling and Substitution of coefficients. *WSEAS Transaction on Signal Processing*, Vol.15, 2019,pp.114-120.

[13] Tiruwa S, Yadav R. Comparing Various Filtering Techniques for Reducing Noise in MRI. *International Conference on Sustainable Energy, Electronics, and Computing Systems (SEEMS),* 2018, pp. 1–5.

[14] Azzeh J, Zahran B, Alqadi Z. Salt and Pepper Noise: Effects and Removal. *JOIV: International Journal on Informatics Visualization*., Vol. 2, No. 4, 2018, pp.252–256.

[15] Hoff M, Andre J, Stewart B. Artifacts in Magnetic Resonance Imaging. *Image Principles, Neck, and the Brain*, 2016, pp. 165–190.

[16] Lee H, Novikov D, and Fieremans E. "Removal of partial Fourier-induced Gibbs (RPG) ringing artifacts in MRI," *Magnetic Resonance in Medicine*, Vol. 86, No. 5, 2021, pp. 2733–2750.

[17] Krupa K, Bekiesińska-Figatowska M. Artifacts in Magnetic Resonance Imaging. *Polish Journal of Radiology,* Vol. 80, 2015, pp. 93-106.

[18] Wilson B, Das J. A Survey of Non-Local Means Based Filters for Image Denoising. *International Journal of Engineering Research & Technology*, Vol. 2, No. 10, 2013, pp. 3768–3771.

[19] Arif F, Akbar M. Empowering Spatial Domain Filters of Digital Image Processing with IFE Tool. *In 8th International Multitopic Conference, Proceedings on INMIC,* 2004, pp. 36–40.

[20] Mehmood R, and Kaur A. "Modified Difference Squared Image Based Non-Local Means Filter," 2020, pp. 1–7.

[21] Shreyamsha B. Image Denoising Based on Non-Local Means Filter and its Method Noise Thresholding. *Signal Image Video Processing,* Vol. 7, No. 6, 2013, pp. 1211–1227.

[22] Dewangan S, Sharma A. Image Smoothening and Sharpening Using Frequency Domain Filtering Technique. *International Journal of Emerging Technologies in Engineering Research(IJETER)*, Vol. 5, No. 4, 2017, pp. 169–174.

[23] Mishro P, Agrawal S, Panda R, and Abraham A, "A Survey on State-of-the-Art Denoising Techniques for Brain Magnetic Resonance Images," *IEEE Reviews in Biomedical Engineering*, Vol. 15, 2021, pp. 184–199.

[24] Karaoğlu O, Bilge H, and Uluer I. "Removal of speckle noises from ultrasound images using five different deep learning networks," *Engineering Science and Technology, an International Journal*, Vol.29, 2022, pp.1-12.

[25] Moreno J, Jaime B, Saucedo S. Towards No-Reference of Peak Signal to Noise Ratio. *International Journal of Advanced Computer Science and Applications*, Vol. 4, No. 1, 2013, pp.122-130.

[26] Huang Y, Song R, Xu K, Ye X, Li C, and Chen X, "Deep learning-based inverse scattering with structural similarity loss functions," *IEEE Sensors Journal*, Vol. 21, No. 4, 2020, pp. 4900–4907.

[27] Siemens Healthineers, Dicom Images, https://www.healthcare.siemens.com/magnetic resonance-imaging[Feb. 2022].